

An automatic approach for urban land-cover classification from Landsat-8 OLI data

Erzhu Li, Peijun Du, Alim Samat, Junshi Xia & Meiqin Che

To cite this article: Erzhu Li, Peijun Du, Alim Samat, Junshi Xia & Meiqin Che (2015) An automatic approach for urban land-cover classification from Landsat-8 OLI data, International Journal of Remote Sensing, 36:24, 5983-6007, DOI: [10.1080/01431161.2015.1109726](https://doi.org/10.1080/01431161.2015.1109726)

To link to this article: <https://doi.org/10.1080/01431161.2015.1109726>



Published online: 24 Nov 2015.



Submit your article to this journal 



Article views: 912



View Crossmark data 



Citing articles: 11 View citing articles 

An automatic approach for urban land-cover classification from Landsat-8 OLI data

Erzhu Li^{a,b}, Peijun Du^{a,b,c*}, Alim Samat^{a,b}, Junshi Xia^{a,b}, and Meiqin Che^{a,b}

^aKey Laboratory for Satellite Mapping Technology and Applications of State Administration of Surveying, Mapping and Geoinformation of China, Nanjing University, Nanjing, China; ^bJiangsu Provincial Key Laboratory of Geographic Information Science and Technology, Nanjing University, Nanjing 210023, China; ^cJiangsu Centre for Collaborative Innovation in Geographical Information Resource Development and Application, Nanjing University, Nanjing 210023, China

(Received 11 March 2015; accepted 2 October 2015)

Due to the lack of clear shape, texture characteristics, and abundant spectral or spatial information of urban objects, traditional per-/sub-pixel analysis and interpretation for moderate-resolution-remote sensing data are always confused by such shortcomings as dependence on special skills, requirements to a priori knowledge and training samples, complex process, time-consuming and subjective operations, etc.. In order to alleviate such disadvantages, an automatic approach is proposed to classify vegetation, water, impervious surface areas (dark and bright), and bare land from the Operational Land Imager (OLI) sensor data of Landsat-8 in urban areas, which can be employed by common users to automatically obtain land-cover maps for urban applications. In detail, a preliminary classification result is achieved based on a new vegetation and water masking index (VWMI), the normalized difference vegetation index (NDVI), and a new normalized difference bare land index (NDBLI), which are acquired automatically from the remote-sensing images based on available knowledge of spectral properties. VWMI is designed to extract vegetation and water information together with a simpler threshold, while NDBLI is developed to identify dark impervious surfaces and bare land in this work. A modification strategy is further proposed to improve preliminary classification results by a linear model. For this purpose, a stable sample selection method based on the histogram is developed to select training samples from the preliminary classification result and to build a non-linear support vector machine (SVM) model to reclassify the classes. For validation and comparison purposes, the proposed approach is evaluated via experiments with real OLI data of two study areas, Nanjing and Ordos. The results demonstrate that the approach is effective in automatically obtaining urban land-cover classification maps from OLI data for thematic analysis.

1. Introduction

Land-use/land-cover (LULC) information is essential for regional and local planning and urban monitoring and management (Crainic, Ricciardi, and Storchi 2009; Flötteröd, Bierlaire, and Nagel 2011; Chen et al. 2006). However, due to the unprecedented global scale and rate of urbanization, it is hard to perfectly plan and precisely forecast urban changes or trends in development over the space–time continuum without detailed and time series LULC information (Dewan and Yamaguchi 2009). Traditional acquisition of LULC information often takes several months or years, which is impractical when

*Corresponding author. Email: dupjrs@126.com

acquiring up-to-date LULC information. Therefore, it is highly desirable to develop a quick, efficient, and reliable way to collect such information.

Remote sensing has been proved an efficient and potential technique for monitoring the spatial distribution and changes in LULC from local to global scales (Loveland et al. 2000; Foody 2002). Numerous methods have been proposed to extract LULC information or class-specific (e.g. vegetation, built-up, road, and urban impervious surfaces) from remote-sensing images (Melgani and Bruzzone 2004; Lu and Weng 2007; Friedl et al. 2010; Yu et al. 2006; Plaza et al. 2009; Varshney and Rajesh 2014). Due to the rapid development of sensors, there are many choices available for remote-sensing imagery in practical applications, such as medium-resolution multispectral imagery (e.g. Landsat Thematic Mapper (TM) and Enhanced Thematic Mapper Plus (ETM+)) (Yusuf, Pradhan, and Idrees 2014; Song et al. 2015), hyperspectral imagery (e.g. AVIRIS and Hyperion) (Dopido et al. 2014; Jia et al. 2014), high-spatial resolution imagery (e.g. QuickBird, IKONOS, and Spot-5) (Powers et al. 2015), and SAR imagery (e.g. Envisat ASAR and TerraSAR) (Kayabol 2015). Many studies have been carried out on fusing multi-sensor data to improve the accuracy of information extraction (Song et al. 2015; Zhang, Zhang, and Lin 2014).

According to the type of object to be investigated, approaches to land-cover information extraction are often divided into pixel-based, object-oriented, and sub-pixel (Lu and Weng 2007; Melgani and Bruzzone 2004; Bioucas-Dias et al. 2012; Yu et al. 2006). Besides, some spectral approaches (e.g. index-based and multi-temporal image analysis methods) are commonly suited for moderate-resolution data such as Landsat TM and ETM+ data sets. For example, the United States Geological Survey (USGS) has developed a multi-temporal national LULC data set with the help of Landsat TM/ETM+ imagery (Yang et al. 2001). Compared with hyperspectral or high-resolution imagery, medium-resolution data with few spectral bands and lower spatial resolution do not provide clear shape, texture characteristics, and other abundant spectral or spatial information of urban objects (Weng, Hu, and Liu 2009). In this case, it is difficult to produce high-precision land-cover classification results using the aforementioned supervised, object-oriented, or sub-pixel approaches over a large area in an efficient way. However, there are many long-term series moderate-resolution images available, such as data collected from the Landsat-1 (from 23 July 1972) to Landsat-8 (from 11 February 2013) multispectral sensors. Other similar earth observation programs (e.g. HJ-1 A/B, CBERS-4) are still under development. Therefore, extracting LULC information remains a challenge in regard to the application of such data.

It has been proved that pixel-based and sub-pixel methods are always considered a complicated, computationally intensive, and sometimes subjective operation. Particularly when applied to a large geographic area (Somers et al. 2011), many problems (training sample selection, endmember selection, etc.) decrease their practicability. Object-oriented methods are more appropriate for high-resolution imagery because of the key requirement for spatial information (Plaza et al. 2009). In comparison, spectral indices have apparent advantages due to their easy implementation and convenience in practice, and index-based classification methods do not require training samples and endmembers. A wealth of indices has been designed to quantify the biophysical characteristics of the earth's surface, the best known being the normalized difference vegetation index (NDVI) (Crippen 1990). Other commonly used indices include the normalized difference water index (NDWI), the modified normalized difference water index (MNDWI) (Gao 1996; Xu 2006), the soil adjusted vegetation

index (SAVI) (Huete 1988), and the normalized difference built-up index (NDBI) (Zha, Gao, and Ni 2003). Although these indices are effective in various applications, they suffer from the same limitations of highlighting one specific land-cover type (e.g. vegetation, water, built-up) and confusion in addressing some land-cover types such as impervious surface and bare land in urban areas. In order to resolve this problem, new and/or improved indices have been developed (He et al. 2010; Liu et al. 2014; Deng and Wu 2012; As-Syakur et al. 2012; Zhou et al. 2014). For instance, the biophysical composition index (BCI) is newly proposed for the derivation of urban biophysical composition (Deng and Wu 2012). These approaches require many given index thresholds varying with collection time and coverage of images for different land-cover types. Moreover, the aforementioned indices are aimed at distinguishing different land-cover types by a linear model. For instance, NDVI is designed in regard to the fact that vegetation has overwhelming values than other types, which ensures that an appropriate value can filter out non-vegetation types. However, it must be recognized that some classes significantly confused are not linearly separated.

Therefore, specifically targeting Landsat-8 data, this study aims to find a method to combine the advantages of spectral indices and machine learning to overcome the drawbacks of spectral index-based methods, and to improve the availability of remote-sensing images. This will help researchers and other users to obtain the required land-cover information quickly from OLI data, which is needed particularly for users lacking sufficient knowledge and skills of remote sensing. The objectives of this article are (1) proposing a simple and effective method of producing initial classification result in urban areas; and (2) using a machine learning classifier trained by automatic selection of training samples from initial classification results to improve those results.

2. Study areas and data sets

The main urban areas of Nanjing and Ordos in China (see Figure 1) are selected as typical study areas. Nanjing, the capital of Jiangsu Province is located at $31^{\circ}14' - 32^{\circ}36'$ N and $118^{\circ}22' - 119^{\circ}14'$ E, with a total area of 6587 km^2 including 653 km^2 of urban area. Dominant land-cover types include agricultural, industrial, forest, grassland, and urban. Besides, the longest inland river in China, the Yangtze, flows through the whole territory, with the urban district located along the river. The terrain is flat and the area has a subtropical monsoon climate characterized by abundant rainfall. Therefore, there is a high level of vegetation coverage.

Ordos in Inner Mongolia is a new and important city that has developed following China's reforms in opening up to the outside world. It is located at $37^{\circ}41' - 40^{\circ}51'$ N and $106^{\circ}42' - 111^{\circ}31'$ E, and covers an area of $86,752 \text{ km}^2$ including 134 km^2 of urban area. The dominant land-cover types include shrub, grassland, agricultural, wasteland, desert, stream, and urban. There are varied landforms, mainly alluvial plain, plateau, hill, and gully. Due to the overwhelming influence of the temperate continental climate, the climate of this region is dry and rainless. As a result, there is little dispersal of vegetation cover.

This research is developed especially for Landsat-8 OLI data. Landsat-8 carries two sensors, the Operational Land Imager (OLI) sensor and the Thermal Infrared Sensor (TIRS). Compared with previous sensors TM and ETM+, the OLI sensor includes six refined heritage bands including TM and ETM+, along with two new spectral bands: a deep blue band designed for coastal/aerosol studies and a shortwave infrared band for cirrus detection. A more detailed description of the Landsat-8 OLI sensor is shown in Table 1.

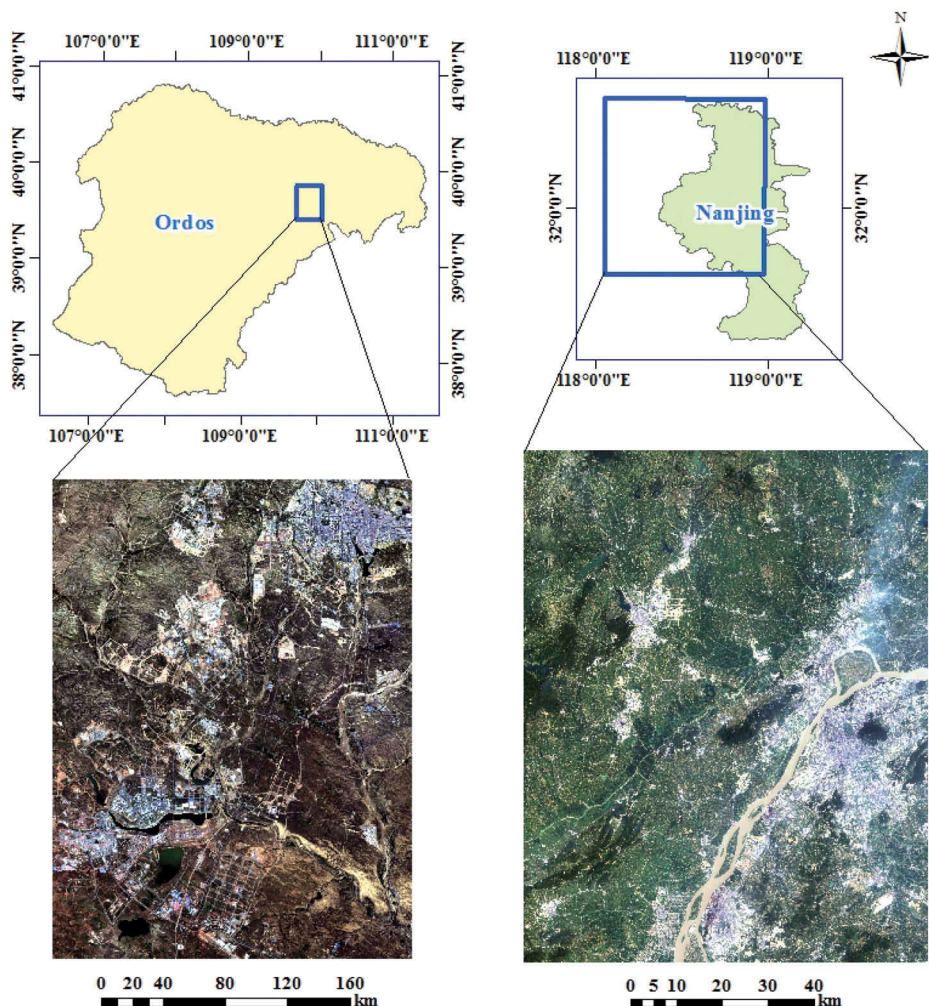


Figure 1. Location of the study areas and the true colour maps of experimental data.

Table 1. Detailed information on Landsat-8 OLI sensor.

Channel	Band number	Wavelength (μm)	Resolution (m)
Coastal aerosol	1	0.433–0.453	30
Blue	2	0.450–0.515	30
Green	3	0.525–0.600	30
Red	4	0.630–0.680	30
NIR	5	0.845–0.885	30
SWIR1	6	1.560–1.660	30
SWIR2	7	2.100–2.300	30
Panchromatic	8	0.500–0.680	15
Cirrus	9	1.360–1.390	30

Table 2. Detailed information on experimental OLI data sets.

Study area	Path/row	Acquisition time
Nanjing	120/38	11 August 2013
Ordos	127/33	15 August 2014

The two experimental OLI images (<http://earthexplorer.usgs.gov/>) covering the main urban areas of Nanjing and Ordos are employed to evaluate the proposed approach. More detailed information on these images is shown in Table 2. In this research, multispectral bands 1–7 are used. Surface reflectance of the OLI data was corrected through an atmospheric correction procedure using the Fast Line-of-sight Atmospheric Analysis of Spectral Hypercubes (FLAASH) model (Kayadibi and Aydal 2013), supported by Environment for Visualizing Images (ENVI) software. The Interactive Data Language-based tool imageSVM (www.hu-geomatics.de) was employed to train the support vector machine (SVM) classification model, and the required parameters (C and γ) were determined by cross-validation supported by this tool. Because imageSVM runs in ENVI software, all processes were completed by this method.

3. Proposed approach

In urban areas, vegetation, water, bare land, and impervious surfaces are always considered as essential land-cover types (Deng and Wu 2012; Ridd 1995). Impervious surfaces include mainly urban residential, commercial, and industrial, etc. Vegetation consists of grass, tree, and farmland in urban areas. Other land-cover types, including farmland without crop covering, bare soil in building areas, and semi-bare soil, are merged into bare land. The main purpose of this study is to develop a more efficient method to extract the four urban land cover classes (vegetation, water, bare land, and impervious surfaces) from OLI data. For this purpose, an automatic classification approach is introduced.

In the process of developing our methods, pure pixels of the four land-cover types are collected through visual interpretation of the OLI data with the help of high-resolution satellite images from Google Earth close to the corresponding dates. For accurate analysis of impervious surfaces, these were divided into bright and dark impervious surfaces. Bright imperviousness has higher reflectivity in the visible light range and is visually displayed as bright tones in remote-sensing images. Newly built concrete surfaces, ceramic tiles, and sheet metal, etc. are all classified as bright impervious surface and are quite common in an urban environment. Conversely, dark impervious surfaces mainly include asphalt, old concrete, and dense buildings, etc., appearing as dark tones in remote-sensing images.

3.1. Vegetation and water extraction

According to the literature, NDVI and MNDWI are frequently and successfully employed to extract vegetation and water information (Mozumder, Tripathi, and Tipdecho 2014; Zhang et al. 2015; Xu 2006). In general, a series of empirical variable values usually requires pre-setting during the extraction process based on NDVI and MNDWI. In order to facilitate the process of extracting vegetation and water with

simpler and fewer empirical values, a newly derived index based on NDVI and MNDWI, namely the vegetation and water masking index (VWMI), is developed.

Generally, vegetation has higher NDVI values than other land-cover types, the value for water is less than zero in general, and others (e.g. impervious surfaces and bare land) show variable ranges. With regard to the shortwave infrared reflectance (SWIR1) band that is used to develop NDBI for built-up extraction, non-vegetation land covers have higher values than vegetation except for water, which absorbs almost all shortwave infrared radiation. Therefore, NDVI and SWIR1 may be suitable for discriminating vegetation and water information from other land-cover types. In this case, values of the SWIR1 band should be normalized to match the range of NDVI from -1 to $+1$.

Figure 2 presents the feature space scatterplots of NDVI and the normalized SWIR1 band with typical urban land-cover types from OLI data for Nanjing. From this figure, it can be seen that the normalized SWIR1 values of bright/dark impervious surface and bare land are higher than their NDVI values while vegetation has an inverse result, and the normalized SWIR1 and NDVI values of water are less than or equal to zero. In this figure, bright/dark impervious surface and bare land are above the two diagonal lines, and water and vegetation below. This means that the normalized SWIR1 values of bare land and impervious surface are higher than their NDVI values. However, because vegetation and water have an inverse relationship, VWMI can be defined as

$$\text{VWMI} = \frac{(\text{NDVI}) - N_{\text{SWIR1}}}{(\text{NDVI}) + N_{\text{SWIR1}}}, \quad (1)$$

$$\text{NDVI} = \frac{\rho_{\text{NIR}} - \rho_{\text{Red}}}{\rho_{\text{NIR}} + \rho_{\text{Red}}}, \quad (2)$$

where N_{SWIR1} denotes the normalized values of SWIR1, and ρ_{NIR} and ρ_{Red} are the reflectance values of the near-infrared and red spectral bands, respectively.

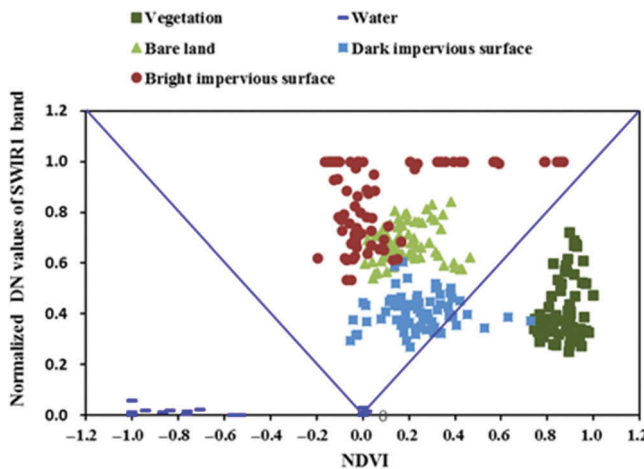


Figure 2. Feature space scatterplots of NDVI and normalized SWIR1 band with typical urban land-cover types from OLI data for Nanjing.

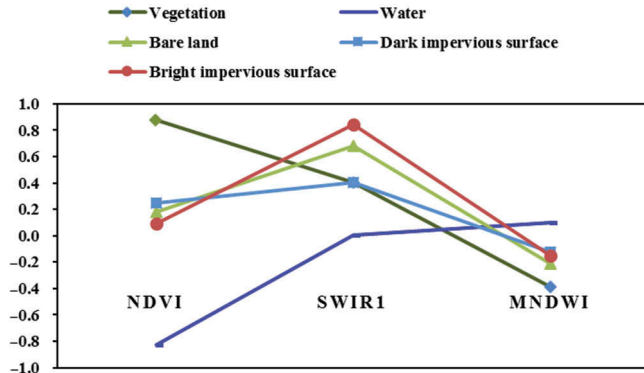


Figure 3. Profiles of NDVI, normalized SWIR1 band, and MNDWI with typical urban land-cover types from OLI data for Nanjing.

From the VWMI calculated according to Equation (1), a simpler threshold zero can be used to extract vegetation and water together. While as shown in Figure 2, some NDVI and SWIR1 values for water are equal to zero, to ensure that all values of VWMI limited, MNDWI (Xu 2006) is employed to modify the model to Equation (3). From the relationships among NDVI, normalized SWIR1, and MNDWI shown in Figure 3, the VWMI values of water and vegetation calculated according to Equation (3) are higher than zero but the values of other parameters may change from negative to positive due to their lower MNDWI. Therefore, the following criterion is designed for MNDWI: if the MNDWI value of a pixel is less than -0.05 , then this is taken as equal to -0.05 ; and if the value is more than 0.05 it is taken as equal to 0.05 . This ensures that water and vegetation have positive MNDWI values while other parameters have negative values:

$$\text{VWMI} = \frac{(\text{NDVI}) - N_{\text{SWIR1}} - (\text{MNDWI})}{(\text{NDVI}) + N_{\text{SWIR1}} - (\text{MNDWI})}, \quad (3)$$

$$\text{MNDWI} = \frac{\rho_{\text{Green}} - \rho_{\text{SWIR}}}{\rho_{\text{Green}} + \rho_{\text{SWIR}}}, \quad (4)$$

where ρ_{Green} and ρ_{SWIR} are the reflectance values of the green and shortwave infrared spectral bands, respectively. SWIR1 is used to calculate the MNDWI index for OLI data.

After extracting vegetation and water information together, it is then simple to distinguish them by NDVI. In fact, NDVI values for vegetation are much higher than zero while water values are much lower (Xu 2006). Thus a positive NDVI value such as 0.2 distinguishes vegetation from water (Chen et al. 2006).

3.2. Impervious surface and bare land extraction

Mapping impervious surfaces at per-pixel level is actually a classification task because these consist of various land-cover materials which are always subdivided into dark (e.g. asphalt, old concrete, and dense buildings) and bright impervious surfaces (e.g. metal, new concrete, and plastic) (Deng and Wu 2012). For multispectral data, dark or bright

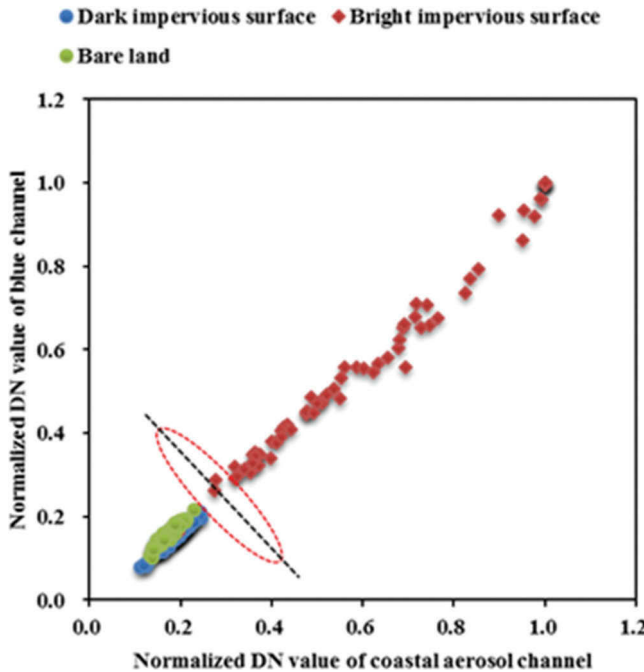


Figure 4. Feature space scatterplots of coastal aerosol and blue bands with three typical urban land-cover types from OLI data for Nanjing.

impervious surface and bare land share similar spectral and spatial characteristics in urban areas, resulting in their separation being problematic. In order to successfully extract them, a more obviously diverse feature space needs to be found. As shown in Figure 4, the normalized values of bright impervious surfaces are obviously higher than those of dark impervious surfaces and bare land in the coastal aerosol and blue bands.

Therefore, normalized coastal aerosol and blue bands are recoded to create a bright impervious surface binary (BISB) image according to Equation (5), with only bright impervious surfaces having positive values:

$$\text{BISB} = \begin{cases} 1, & \frac{N_{\text{Coastal}} + N_{\text{Blue}}}{2} > \alpha, \\ 0, & \text{Others} \end{cases} \quad (5)$$

where N_{Coastal} and N_{Blue} are the normalized values of the coastal aerosol and blue bands, respectively.

After extracting bright imperviousness, an interest distribution in space of the coastal aerosol and blue channels is found for dark impervious surfaces and bare land (see Figure 5), where these are distinguished by a linear model represented by the red line, but the ideal model is the diagonal represented by the blue line. In Figure 5(b) the separability between dark impervious surfaces and bare land is finer in the the green and coastal aerosol bands. Moreover, a preferable linear model approaching the ideal completes the classification work. In practice, the ideal model without varied model parameters in the green and coastal aerosol bands can be conveniently, and therefore a new

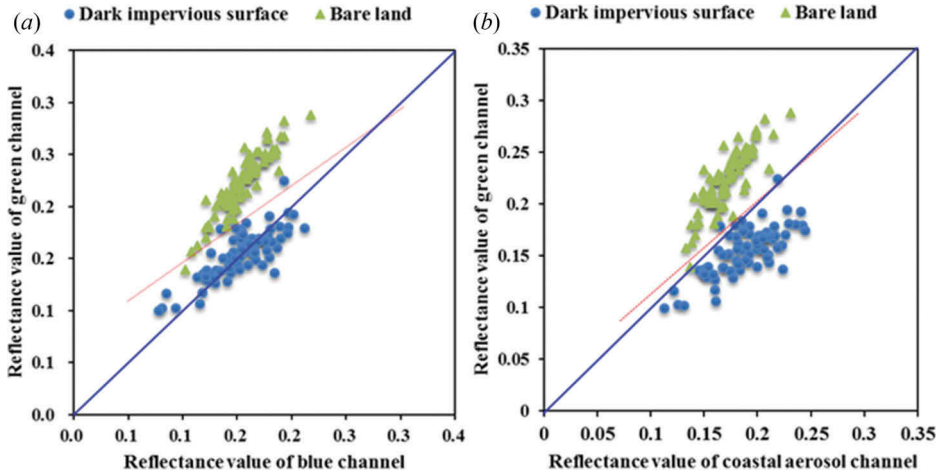


Figure 5. Feature space scatterplots of green and blue or coastal aerosol bands from OLI data for Nanjing.

index, the normalized difference bare land index (NDBLI), is developed to extract bare land from dark impervious surfaces:

$$\text{NDBLI} = \frac{\rho_{\text{Green}} - \rho_{\text{Coastal}}}{\rho_{\text{Green}} + \rho_{\text{Coastal}}}, \quad (6)$$

where ρ_{Green} and ρ_{Coastal} denote the reflectance of the green and coastal aerosol bands, respectively. In general, a threshold close to zero separates bare land from dark impervious surfaces.

3.3. Modification of land-cover classification

As mentioned before, an automatic approach based on spectral indices is introduced initially to execute the classification task. Many spectral index-based approaches attempt to identify land-cover types using a linear model, but much land cover in urban area consists of various materials and accurate separation using a linear model is problematic. Therefore, a non-linear model may be a more appropriate choice for accurate classification and the most widely used non-linear classification models are supervised methods. In this study, a non-linear SVM (Chang and Lin 2011) is used to modify the preliminary classification results.

For a supervised method, training samples must be selected to build a classifier. This is deemed to be a consuming thing, especially for large geographic areas (e.g. large urban areas). In this study, a preliminary classification result was achieved based on the indices introduced above. The training samples were automatically selected from the primary classification result. However, the next issue is how to select precise and effective samples for training. In the literature, random selection is frequently employed and has proved a simple but unstable method (Tan et al. 2014). In order to circumvent its disadvantages, a new sample selection strategy is developed and applied in this study.

In regard to training samples, it is best to represent the distribution of the classified data in the feature space, and histograms are frequently used to describe this. For one class of primary classification result, all samples of this class are first transformed to a

new space according to Equations (7)–(8), and the new space is used for depicting the spectral curve shape of the samples. Next, samples with the same spectral curve shape are clustered into one class and finally the samples of each clustered class are enumerated to yield the histogram for that class. The training samples of this class are randomly selected in proportion based on this histogram, which means that more samples are selected in one clustered class with higher values of histogram statistics.

Let $X = (x^1, x^2, \dots, x^m) \in \mathbb{R}^n$ denote one class with m samples and n bands, and $x^i = \{x_1^i, x_2^i, \dots, x_n^i\}$ denote one sample with n bands. Let $Y = (y^1, y^2, \dots, y^m) \in \mathbb{R}^{n(n-1)/2}$ denote spectral curve shape vectors of the m samples, and $y^i = \{y_1^i, y_2^i, \dots, y_{n(n-1)/2}^i\}$ is a spectral curve vector. y^i is calculated by Equations (7)–(8) as follows, where $\emptyset(z)$ is a binary function:

$$y^i = \left\{ \emptyset(x_q^i - x_p^i) \mid p < q; p, q = 1, 2, \dots, n \right\}, \quad (7)$$

$$\emptyset(z) = \begin{cases} 1, & z \geq 0 \\ 0, & z < 0 \end{cases}. \quad (8)$$

After selecting training samples from the primary classification result of each class, the SVM method is used to train a classifier which will reclassify all samples of the classes, and the reclassified results will be final instead of preliminary.

3.4. Automatic classification framework in urban areas derived from OLI data

The proposed approach, which is based on a group of indices and machine learning, can be summarized by the following steps. First, VWMI is proposed to effectively extract vegetation and water information together, which are then easily separated by NDVI; second, a BISSB image is created to extract the bright impervious surface area; third, NDBLI is developed to identify dark impervious surface area and bare land. Furthermore, in order to improve the classification performance, we adopted a non-linear SVM to reclassify the classes vegetation, water, impervious surface, and bare land. This is an automatic approach with no initial training samples input, the procedure being shown in Figure 6.

As shown in Figure 6, there are five parameters to set but only three parameters are given – threshold α in Equation (5), the threshold of NDBLI for separating bare land and dark impervious surface, and the percentage of training samples selected from the preliminary result. The thresholds of NDVI and VWMI are set to 0.2 and 0, respectively.

4. Experiments and results

In this section, the two OLI data sets introduced in Section 2 are used to evaluate the proposed approach. In order to illustrate its performance, three accuracy measures are employed in the process of accuracy assessment:

- Overall accuracy (OA): the percentage of correctly classified samples.
- Average accuracy (AA): average percentage of correctly classified samples for individual classes.

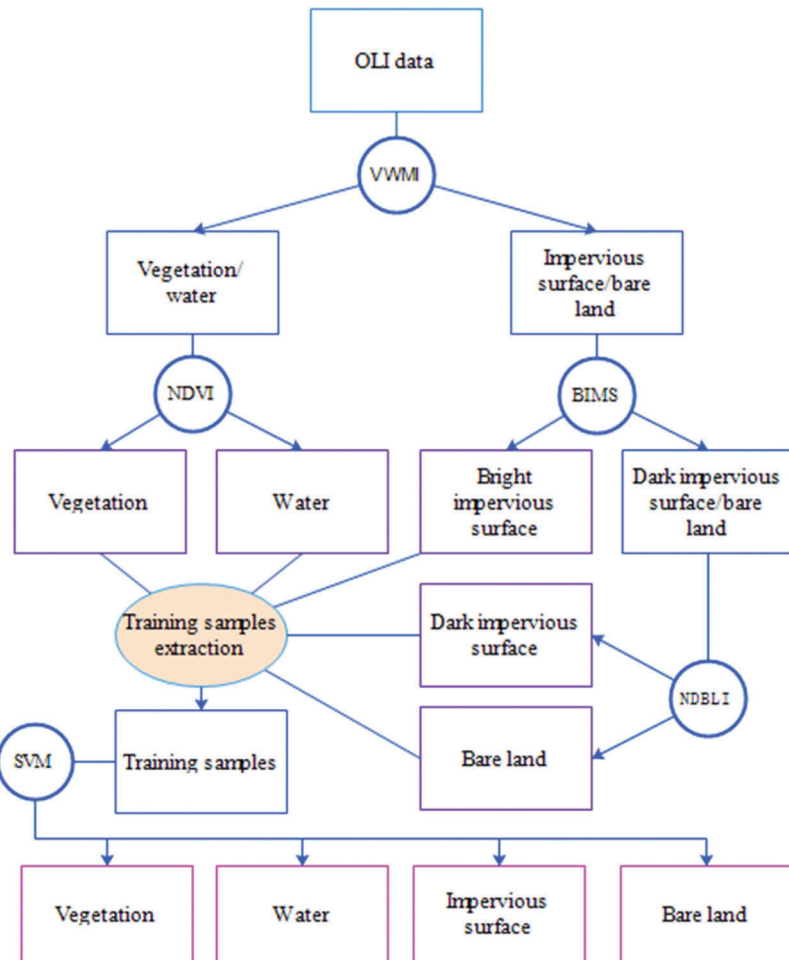


Figure 6. The proposed automatic classification framework.

- Kappa coefficient (κ): the percentage agreement corrected by the level of agreement that would be expected from chance alone.

In addition, reference data are collected through visual interpretation of the OLI data, and high-resolution satellite images from Google Earth close to the corresponding dates are used to help the interpretation. Finally, 4449 and 5279 samples were collected for Nanjing and Ordos, respectively. Note that these reference samples are used only as test samples to evaluate the performance of the proposed approach.

In the following we first present the validation results of new proposed indices then give the classification results of the two study areas using the proposed method. Finally an analysis of parameters is discussed.

4.1. Validation of VWMI and NDBLI

To assess the performance of VWMI and NDBLI in discriminating land-cover types in an urban environment, four other spectral indices – NDVI, NDBI, normalized difference

imperious surface index (NDISI) (Xu 2010), and BCI – were employed for comparison. NDVI is calculated according to Equation (2) and the three other spectral indices are calculated by Equations (9)–(14):

$$\text{NDBI} = \frac{\rho_{\text{SWIR}} - \rho_{\text{NIR}}}{\rho_{\text{SWIR}} + \rho_{\text{NIR}}}, \quad (9)$$

$$\text{NDISI} = \frac{\rho_{\text{TIR}} - ((\text{MNDWI}) + \rho_{\text{NIR}} + \rho_{\text{SWIR}})/3}{\rho_{\text{TIR}} + ((\text{MNDWI}) + \rho_{\text{NIR}} + \rho_{\text{SWIR}})/3}, \quad (10)$$

$$\text{BCI} = \frac{(H + L)/2 - V}{(H + L)/2 + V}, \quad (11)$$

with

$$H = \frac{(\text{TC})_1 - (\text{TC})_{1,\min}}{(\text{TC})_{1,\max} - (\text{TC})_{1,\min}}, \quad (12)$$

$$V = \frac{(\text{TC})_2 - (\text{TC})_{2,\min}}{(\text{TC})_{2,\max} - (\text{TC})_{2,\min}}, \quad (13)$$

$$L = \frac{(\text{TC})_3 - (\text{TC})_{3,\min}}{(\text{TC})_{3,\max} - (\text{TC})_{3,\min}}, \quad (14)$$

where ρ_{NIR} , ρ_{SWIR} , and ρ_{TIR} are near-infrared, shortwave infrared, and thermal infrared spectral bands, respectively. $(\text{TC})_i$ ($i = 1, 2$, and 3) are the first three TC components calculated by tasseled cap (TC) transformation (Kauth and Thomas 1976), and $(\text{TC})_{i,\min}$ and $(\text{TC})_{i,\max}$ are the minimum and maximum values of the corresponding TC component, respectively.

Figure 7 shows the OLI data for Nanjing and resultant indices. With the aim of examining the performance of VWMI and NDBLI, comparative analyses with four other parameters (NDVI, NDBI, NDISI, and BCI) were performed based on mean and standard deviation values (see Table 3). In addition, the separability measurement J–M distance(Swain and Davis 1981) was employed to quantify the degree of separation of two land-cover types with different indices, and the results are reported in Table 4.

As illustrated in Figure 7(e), the VWMI image indicates that water has the highest positive values and is characterized by a white tone while vegetation has the second highest positive values, indicated by a light grey tone. Impervious surface and bare land have a VWMI value less than zero, and are denoted by a dark grey and black, respectively. For the NDBLI image (see Figure 7(f)), bare land and vegetation have the highest values with a light grey tone, impervious surface and water have lower values and appear as medium and dark grey, respectively. The NDVI image indicates obvious distinction between vegetation and water, while impervious surface and bare land are visually confused. The NDBI image shows that impervious surface and bare land have the highest positive values, but are also visually confused. Water has the highest values according to the NDISI image (see Figure 7(c)), with bare land and impervious surface

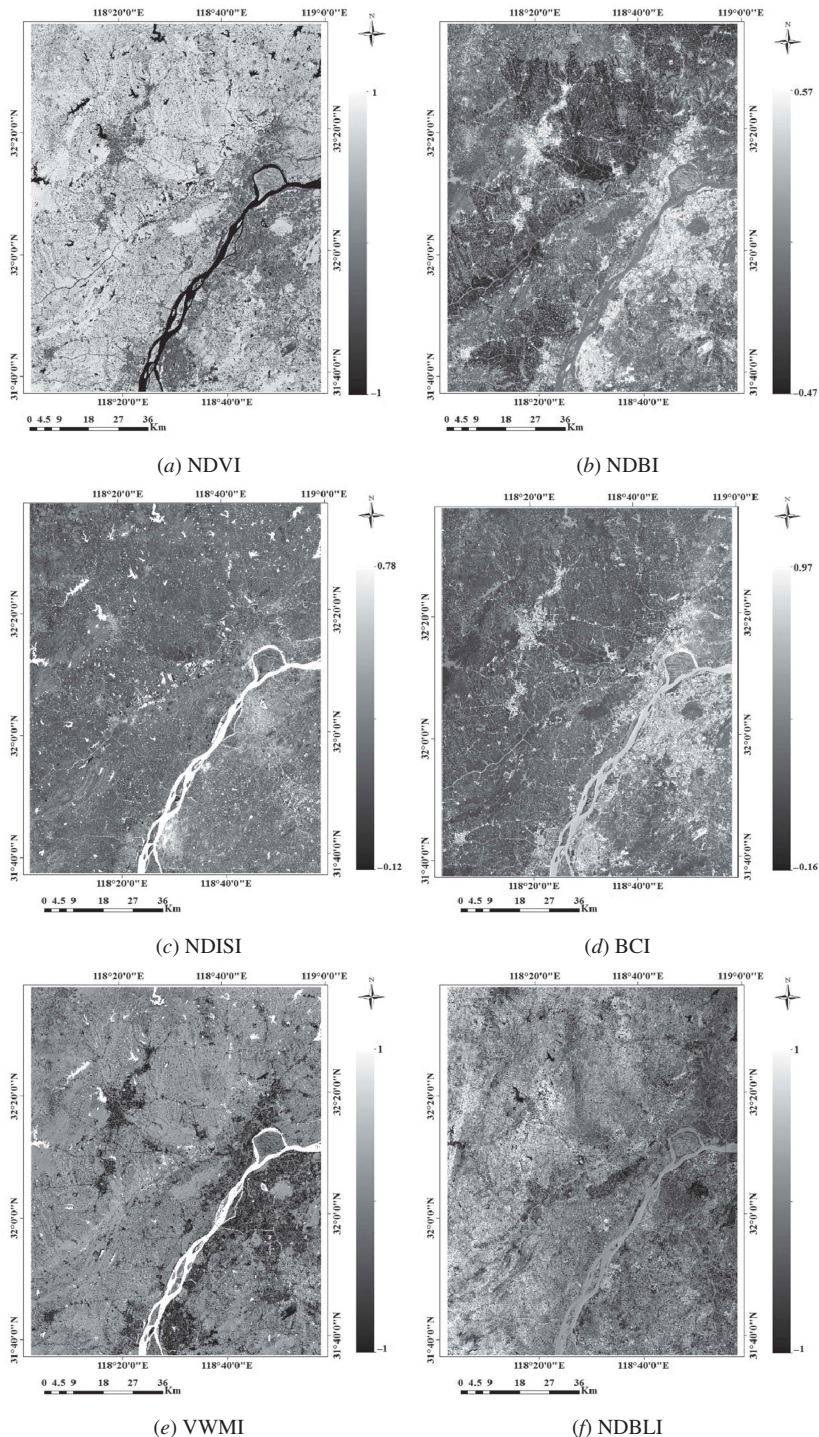


Figure 7. Comparisons of OLI indices (Nanjing). (a) NDVI, (b) NDBI, (c) NDISI, (d) BCI, (e) VWMI, (f) NDBLI.

Table 3. Statistics of different land covers with different indices (Nanjing).

Class		NDVI	NDBI	NDISI	BCI	VWMI	NDBLI
Vegetation	Mean	0.875	-0.264	0.440	0.002	0.378	-0.055
	Std. dev.	0.061	0.053	0.063	0.032	0.113	0.131
Water	Mean	-0.830	-0.163	0.727	0.116	0.888	-0.103
	Std. dev.	0.312	0.026	0.011	0.037	0.400	0.231
Dark impervious surface	Mean	0.246	-0.044	0.559	0.145	-0.313	-0.097
	Std. dev.	0.142	0.053	0.029	0.027	0.340	0.053
Bright impervious surface	Mean	0.090	0.033	0.405	0.460	-0.930	-0.105
	Std. dev.	0.265	0.074	0.076	0.179	0.383	0.223
Bare land	Mean	0.181	-0.012	0.463	0.126	-0.603	0.130
	Std. dev.	0.110	0.030	0.027	0.019	0.196	0.037

Table 4. Separability measures between two land-cover types with different indices (Nanjing).

Class	NDVI	NDBI	NDISI	BCI	VWMI	NDBLI
Vegetation & dark impervious surface	1.404	1.330	1.079	1.407	1.178	-
Vegetation & bright impervious surface	1.355	1.366	0.279	1.326	1.378	-
Vegetation & bare land	1.414	1.406	0.591	1.371	1.408	-
Water & dark impervious surface	1.361	1.158	1.414	0.481	1.209	-
Water & bright impervious surface	1.199	1.289	1.412	1.218	1.365	-
Water & bare land	1.404	1.395	1.414	0.466	1.382	-
Dark impervious surface & bare land	0.309	0.526	1.243	0.467	-	1.382

Note: The symbol ‘-’ denotes that the J–M distance was not calculated.

shown by a similar grey tone. In the BCI image (see Figure 7(d)), water, bare land, and impervious surface are shown in a tone of mid-grey, while vegetation with the lowest values appears as dark grey.

According to the discussion above, impervious surface and bare land are the most difficult targets for the previously proposed indices. In contrast, the newly proposed index NDBLI is visually competent. In order to quantify the varying separability of different land covers with different indices, mean and standard deviation are calculated (see Table 3). The statistics show that vegetation and water have the best separability with NDVI while NDBLI has better statistic characteristics for impervious surface and bare land. NDBLI has better separability for impervious surface and bare land than other indices. Vegetation and water have positive values of VWMI, with impervious surface and bare land having negative values. Specifically, there is an obvious difference between the positive and negative groups separated in regard to VWMI.

In this research we investigated the separability between pure pixels of two land covers by quantification using J–M distance measurement with different indices. The J–M distance indicates the separability between two classes, with a value less than 1.00 indicating that the two classes are poorly separable. Further, values higher than 1.38 indicate a high degree of separability, and values between 1.00 and 1.38 indicate that the two classes are moderately separable (Thomas *et al.* 1987). As shown in Table 4, for difficult targets, dark impervious and bare land are moderately separated for NDISI, but NDBLI showed a better performance. VWMI proved efficient in discriminating vegetation and water from other land covers listed in Table 4, even though it did not perform better

than all others. Moreover, as illustrated above, vegetation and water have positive values of VWMI and the others negative.

As a further comparison, the second experimental data set was employed for further analysis. The derived indices (see [Figure 8](#)) indicate similar results compared to the first set. In addition, impervious surface and bare land are displayed with more significant visual difference in the NDBLI image (see [Figure 8\(f\)](#)), due to the wide distribution of bare land in this study area.

A detailed analysis of the statistics of different land-cover types with different indices indicates that impervious surface and bare land result in significant confusion for NDVI, NDBI, BCI, and VWMI (see [Table 5](#)). However, NDISI and NDBLI show better performance in separating bare land from impervious surface. A further analysis shows that NDISI values of bare land are higher than those of bright impervious surface and lower than those of dark impervious. For NDBLI, the values of bare land are higher than those of bright and dark impervious surfaces, and moreover they could be separated by a threshold close to zero. VWMI shows similar statistical characteristics compared to the first data.

The separability measures results are reported in [Table 6](#). Similar conclusions are drawn that vegetation and water could be better separated from impervious surface and bare land through VWMI. Bare land and dark impervious surface could be moderately separated with NDISI and NDBLI, and NDBLI shows the best performance.

In summary, the newly proposed indices VWMI and NDBLI have particular advantages compared with previously commonly used indices. According to comparison of both experiments, VWMI and NDBLI not only exhibit good separability for different land-cover types, but also have an advantage in terms of threshold determining the separation of different land-cover types.

4.2. Results for Nanjing

In this subsection, we show the results obtained when the proposed approach is applied for the first OLI data of Nanjing. For comparable analysis, a supervised classification result based on SVM with manually labelled training samples is conducted (see SVM in [Table 7](#)). As a result, two classification results are achieved by the proposed approach with or without the modification procedure, respectively. The preliminary result is achieved without the modification procedure, and the SVM-a result is modified. In this experiment, the threshold α in Equation (5) is set to 0.4, the threshold of NDBLI is set to 0, and 0.05% of samples are selected from the preliminary classification result including five classes to train a SVM classifier. The results of dark and bright impervious surface are merged into impervious surface as the final imperviousness land cover. The input features to be trained and reclassified are multispectral reflectance bands 1–7 of OLI data.

[Table 7](#) presents the experimental results of Nanjing OLI data. According to the results presented in [Table 7](#), vegetation and water have very high class-specific accuracy. In contrast, impervious surface has a lower accuracy and bare land has the lowest accuracy, with its OA only 76.52%, and other accuracy measures are similar. This indicates that impervious surface and bare land are very difficult to identify. With the modification procedure the SVM method is employed to improve accuracy, and the accuracy of bare land is markedly improved to 85.54%. However, there is a small decrease for impervious surface. This is probably due to the fact that some impervious

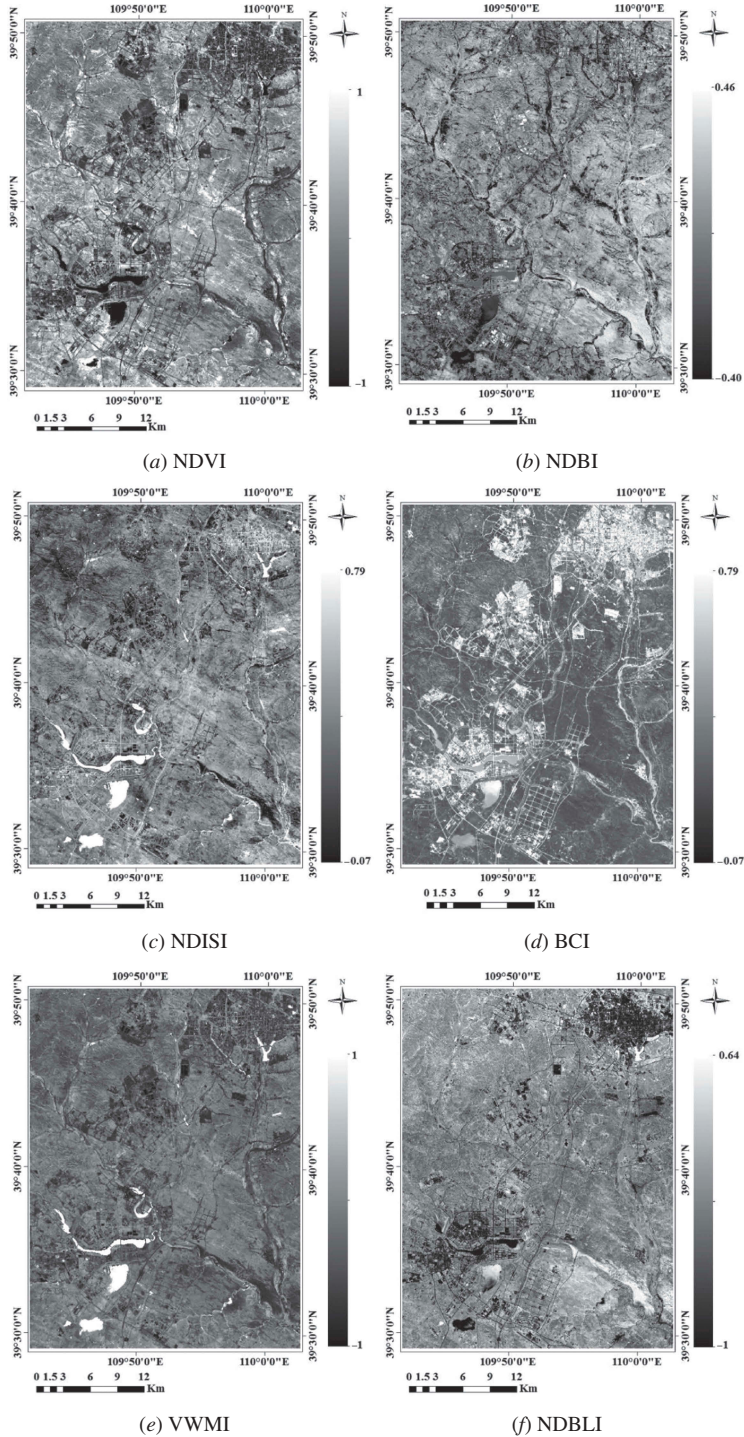


Figure 8. Comparisons of OLI indices (Ordos). (a) NDVI, (b) NDBI, (c) NDISI, (d) BCI, (e) VWMI, (f) NDBLI.

Table 5. Statistics of different land-cover types with different indices (Ordos).

Class		NDVI	NDBI	NDISI	BCI	VWMI	NDBLI
Vegetation	Mean	0.676	-0.182	0.466	-0.291	0.229	0.231
	Std. dev.	0.096	0.062	0.034	0.035	0.144	0.058
Water	Mean	-0.333	-0.095	0.756	-0.129	1.000	0.118
	Std. dev.	0.454	0.067	0.025	0.046	0.000	0.136
Dark impervious surface	Mean	0.059	-0.001	0.556	-0.029	-0.626	0.059
	Std. dev.	0.048	0.032	0.039	0.073	0.206	0.053
Bright impervious surface	Mean	0.186	0.041	0.332	0.179	-0.678	-0.093
	Std. dev.	0.271	0.105	0.084	0.261	0.353	0.228
Bare land	Mean	0.209	0.025	0.429	-0.196	-0.534	0.221
	Std. dev.	0.106	0.024	0.053	0.086	0.234	0.048

Table 6. Separability measures between two land covers with different indices (Ordos).

Class	NDVI	NDBI	NDISI	BCI	VWMI	NDBLI
Vegetation & dark impervious surface	1.414	1.379	1.015	1.369	1.376	-
Vegetation & bright impervious surface	1.108	1.092	1.013	1.241	1.262	-
Vegetation & bare land	1.364	1.362	0.493	0.848	1.313	-
Water & dark impervious surface	1.119	0.909	1.408	0.797	1.414	-
Water & bright impervious surface	0.725	0.769	1.413	1.078	1.414	-
Water & bare land	1.107	1.104	1.414	0.617	1.414	-
Dark impervious surface & bare land	0.927	0.482	1.103	0.913	-	1.202

Note: The symbol ‘-’ denotes that the J-M distance was not calculated.

Table 7. Accuracy assessment results for OLI data of Nanjing.

Class	Test samples	Test accuracy (%)		
		Preliminary result	SVM-a	SVM
Vegetation	1169	100.00	100.00	98.21
Water	1074	99.63	100.00	100.00
Impervious surface	1086	94.57	91.92	85.01
Bare land	1120	76.52	85.54	84.20
κ		0.9023	0.9252	0.8865
OA		92.67	94.45	91.55
AA		92.68	94.37	91.86

surfaces and bare land have very similar spectra while the SVM model is trained based on reflectance bands 1–7 of OLI data. Overall, the accuracy assessment measures increase with modification procedure. In mapping application, the modification result (SVM result) is more practical generally. In contrast, the supervised classification result (SVM) shows lower accuracy, and impervious surface and bare land have significant confusion due to the quality and quantity uncertainty of manually selected training samples.

For better illustration purposes, two typical small regions are selected from the study area shown in Figures 9(b)–(c). Specifically, Figure 9 shows the classification map

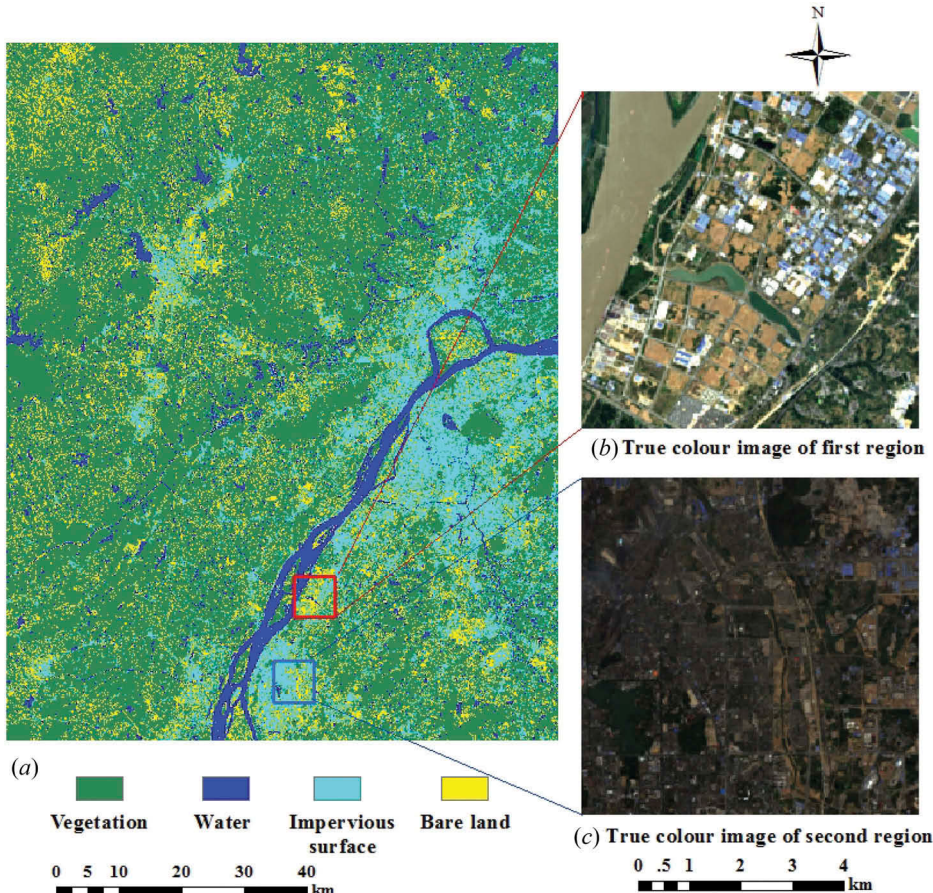


Figure 9. Classification result with SVM modification and two typical regions for OLI data of Nanjing. (a) SVM-a, (b) true colour images of the first region, (c) true colour images of the second region.

obtained by the SVM-a method (see Figure 9(a)) and true colour images of two typical regions. As shown in Figure 9 (b), the first region is a newly developed area, so the main impervious surface is bright imperviousness and bare land in this region is fresh soil. Therefore, these are easily distinguished by the proposed approach either with or without the modification procedure, a good classification result is achieved by the supervised SVM as well, and the results can be seen in Figures 10(a)–(c). For the second region, this is a mature urban area mainly including dark impervious surface and degraded soil that has been bare for a long time, and these are confused visibly as shown in Figure 9(c). In this case, the approach with SVM modification achieves a better result as seen in Figure 10(f). Both vegetation and water show perfect performance. Compared with the results of the proposed methods, the results of bare land and impervious surface obtained by SVM are better than the preliminary results but worse than the SVM-a. This first indicates that a non-linear model is more suitable to separate bare land and impervious surface. Second, the SVM model is sensitive for training samples. Besides, the results (see Figure 10(f)) also show an obvious error in regard to industrial mining land, which is

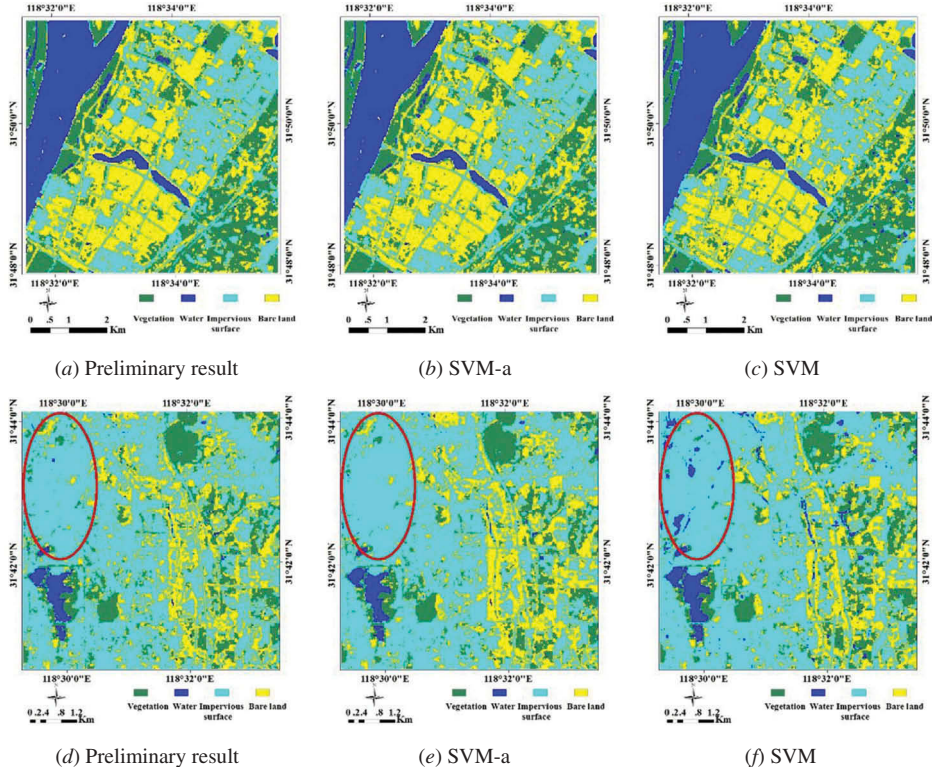


Figure 10. The typical regions of Nanjing and their classification maps of the proposed approach. (a) Preliminary result, (b) SVM-a, (c) SVM, (d) Preliminary result, (e) SVM-a, (f) SVM.

classified as water. For the SVM-a result (see Figure 10(e)), there is little error even when using the same method SVM to build the non-linear classification model. It demonstrates that training samples are the main reason leading to such error. Specifically, some errors occur because of manually selecting only a few training samples or not selecting samples of some special land uses. These are common problems for mapping targets with a supervised method.

4.3. Results for Ordos

Here we provide another test for the proposed approach using the second OLI data for Ordos. In this experiment, the threshold α in Equation (5) is set to 0.4, the threshold of NDBLI is set to 0.1, and 0.5% of samples are selected from preliminary classification results to train the SVM-a model. The results are shown in Table 8. The findings are similar to previous experiments, showing that vegetation and water have very accurate classification results. However, the accuracy of impervious surface is lower than bare land in this experiment, possibly due to the fact that there is much bare land in the built-up areas of Ordos, which are widely dispersed. This increases the difficulty in extracting impervious surface from bare land because of greater numbers of pixels confusing these land covers. Even so, the preliminary result shows good performance in terms of the

Table 8. Accuracy assessment results for OLI data of Ordos.

Class	Test samples	Test accuracy (%)		
		Preliminary result	SVM-a	SVM
Vegetation	1044	97.89	98.15	99.90
Water	1200	99.08	99.33	99.08
Impervious surface	1714	85.69	90.08	88.64
Bare land	1321	92.36	97.49	93.82
κ		0.9099	0.9485	0.9314
OA		93.31	96.19	94.92
AA		93.76	96.27	95.36

accuracy measures. The SVM-a result achieves the highest accuracy, and bare land and impervious surface show better separability for the non-linear model.

Two typical regions of Ordos are shown in Figures 11(b)–(c); these are newly developed areas with many mixed pixels of bare land and impervious surface. The built-up areas are surrounded by bare land, and many patches of bare land are distributed in the built-up areas. Therefore, it is difficult to extract patches of bare land from built-up areas. As shown in Figure 12(f), the patches of bare land are mostly classified into impervious surface by SVM, and this is improved with SVM-a. There is a similar phenomenon in that some errors occur due to manual selection of samples (see Figure 12(c)).

4.4. Parameter analysis

According to the framework described in subsection 3.4, there are three tuning parameters: threshold α in Equation (5) that is set to extract bright impervious surface, the threshold of NDBLI to separate bare land and impervious surface, and the proportion of training samples in the preliminary result.

The parameter α is defined by assessing the brightness of the OLI data, and it is influenced by atmospheric condition at the time of data acquisition. In the experiments, we find that the threshold α could be set on the basis of mean average normalized values of the coastal aerosol and blue bands, and it should be set to a higher value than the mean. For instance, the first experimental data have a mean value of 0.32 and the threshold α is set to 0.4, while the second experimental data have a mean value of 0.24 and the threshold is also set to 0.4. It is notable that α is a variable and is not required to be set precisely, because there is a relatively wide range between bright impervious surface and others as shown in Figure 3. In practice, a value 0.05–0.20 greater than the mean value is suggested to be set.

The NDBLI is a major plus in this study. It provides a better feature space to separate bare land from imperviousness compared with previously developed indices. In the first experimental data, it is set to 0 because of the low number of mixed pixels of bare land and impervious surface. However, it is changed to 0.1 in the second experimental data. This indicates that it is hard to define a constant threshold value, especially for study areas with obvious differences. However, we also find a useful conclusion that the threshold should be set to a value no less than zero, and close to zero if higher than zero.

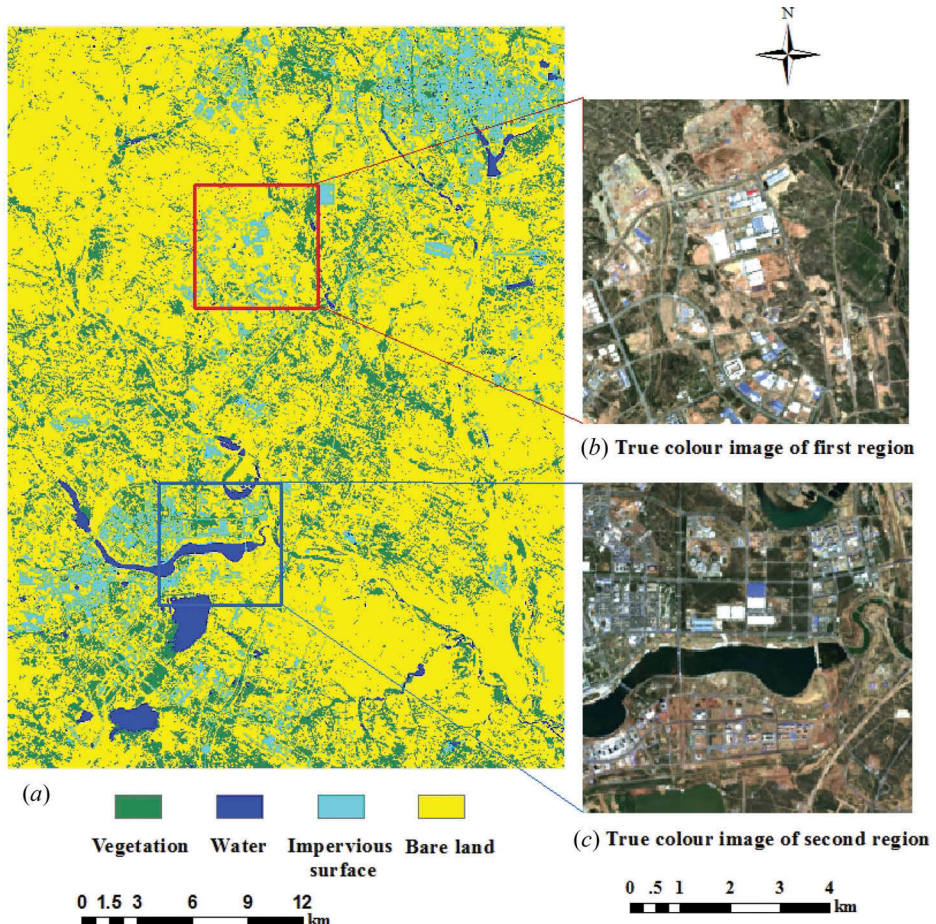


Figure 11. Classification results with SVM modification and two typical regions for OLI data of Ordos. (a) SVM-a, (b) true colour images of the first region, (c) true colour images of the second region.

The proportion of training samples in the preliminary result is used to control the numbers of samples to train a classifier based on the SVM method. In this study, different proportions are selected to evaluate the sensitivity of the proposed approach to this parameter. As shown in Figure 13, the accuracy achieved by the proposed approach is stable with percentage change. This indicates that the selection strategy introduced in subsection 3.3 is effective in describing the data distribution in feature space. In order to save time in training the classifier, a small proportion is suggested to be selected.

5. Conclusions

Urban land-cover mapping is an important task for many researches and applications related to urban planning, environmental management, climate change, and ecological protection, etc., and accurate mapping remains challenging due to the spectral diversity of impervious surfaces in urban areas. This study presents a new automatic classification

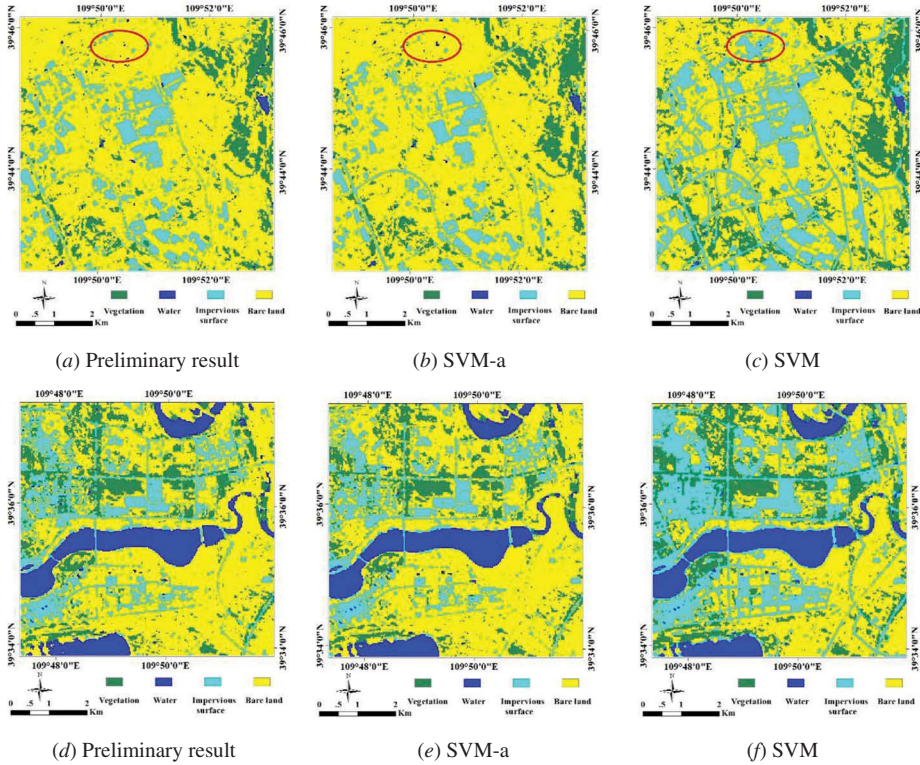


Figure 12. The typical regions of Ordos and their classification maps of the proposed approach. (a) Preliminary result, (b) SVM-a, (c) SVM, (d) Preliminary result, (e) SVM-a, (f) SVM.

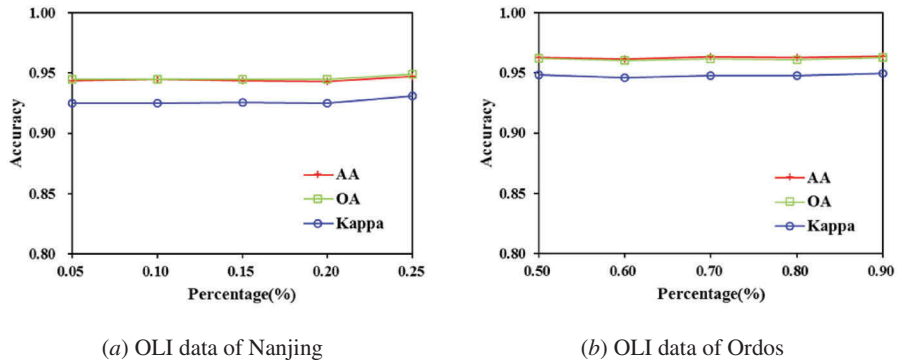


Figure 13. Sensitivity analysis of the proportion of training samples selection.

approach to achieve land-cover mapping of a large urban area based on Landsat-8 OLI data. Compared with traditional methods based on spectral indices, it is a fast and effective method with fewer variable parameters and easy implementation, which is more important in practice especially for users without abundant processing skills in remote sensing. Typical study areas, Nanjing and Ordos, are selected to test the

effectiveness of the approach. The results demonstrate that the approach offers a good performance in terms of three accuracy indices (κ , OA, and AA); it extracted vegetation and water perfectly and distinguished impervious surface and bare land effectively. The information or maps so derived can then be used for various thematic analysis. The proposed approach is developed on OLI data, but may not perform well when applied to other multispectral images. Further studies on other images will be conducted in the near future.

Acknowledgement

The authors would like to thank the Earth Resources Observation and Science Centre (EROS) of the USGS for providing Landsat-8 remote-sensing images.

Disclosure statement

No potential conflict of interest was reported by the authors.

Funding

This study is jointly supported by the Jiangsu Provincial Natural Science Foundation [grant number BK2012018] and the Research Projects of China Geological Survey [grant number 12120113007500]. The authors are also funded by the Priority Academic Program Development of Jiangsu Higher Education Institutions (PAPD) and the Fundamental Research Funds for the Central Universities.

References

- As-Syakur, A. R., I. W. S. Adnyana, I. W. Arthana, and I. W. Nuarsa. 2012. "Enhanced Built-Up and Bareness Index (EBBI) for Mapping Built-Up and Bare Land in an Urban Area." *Remote Sensing* 4 (10): 2957–2970. doi:[10.3390/rs4102957](https://doi.org/10.3390/rs4102957).
- Bioucas-Dias, J. M., A. Plaza, N. Dobigeon, M. Parente, Q. Du, P. Gader, and J. Chanussot. 2012. "Hyperspectral Unmixing Overview: Geometrical, Statistical, and Sparse Regression-Based Approaches." *IEEE Journal of Selected Topics in Applied Earth Observations and Remote Sensing* 5 (2): 354–379. doi:[10.1109/jstas.2012.2194696](https://doi.org/10.1109/jstas.2012.2194696).
- Chang, -C.-C., and C.-J. Lin. 2011. "LIBSVM: A Library for Support Vector Machines." *Acm Transactions on Intelligent Systems and Technology* 2 (3): 1–27. doi:[10.1145/1961189.1961199](https://doi.org/10.1145/1961189.1961199).
- Chen, X.-L., H.-M. Zhao, P.-X. Li, and Z.-Y. Yin. 2006. "Remote Sensing Image-Based Analysis of the Relationship between Urban Heat Island and Land Use/Cover Changes." *Remote Sensing of Environment* 104 (2): 133–146. doi:[10.1016/j.rse.2005.11.016](https://doi.org/10.1016/j.rse.2005.11.016).
- Crainic, T. G., N. Ricciardi, and G. Storchi. 2009. "Models for Evaluating and Planning City Logistics Systems." *Transportation Science* 43 (4): 432–454. doi:[10.1287/trsc.1090.0279](https://doi.org/10.1287/trsc.1090.0279).
- Crippen, R. E. 1990. "Calculating the Vegetation Index Faster." *Remote Sensing of Environment* 34 (1): 71–73. doi:[10.1016/0034-4257\(90\)90085-z](https://doi.org/10.1016/0034-4257(90)90085-z).
- Deng, C., and C. Wu. 2012. "BCI: A Biophysical Composition Index for Remote Sensing of Urban Environments." *Remote Sensing of Environment* 127: 247–259. doi:[10.1016/j.rse.2012.09.009](https://doi.org/10.1016/j.rse.2012.09.009).
- Dewan, A. M., and Y. Yamaguchi. 2009. "Land Use and Land Cover Change in Greater Dhaka, Bangladesh: Using Remote Sensing to Promote Sustainable Urbanization." *Applied Geography* 29 (3): 390–401. doi:[10.1016/j.apgeog.2008.12.005](https://doi.org/10.1016/j.apgeog.2008.12.005).
- Dopido, I., J. Li, P. Gamba, and A. Plaza. 2014. "A New Hybrid Strategy Combining Semisupervised Classification and Unmixing of Hyperspectral Data." *Ieee Journal of Selected Topics in Applied Earth Observations and Remote Sensing* 7 (8): 3619–3629. doi:[10.1109/jstas.2014.2322143](https://doi.org/10.1109/jstas.2014.2322143).
- Flötteröd, G., M. Bierlaire, and K. Nagel. 2011. "Bayesian Demand Calibration for Dynamic Traffic Simulations." *Transportation Science* 45 (4): 541–561. doi:[10.1287/trsc.1100.0367](https://doi.org/10.1287/trsc.1100.0367).

- Foody, G. M. 2002. "Status of Land Cover Classification Accuracy Assessment." *Remote Sensing of Environment* 80 (1): 185–201. doi:[10.1016/s0034-4257\(01\)00295-4](https://doi.org/10.1016/s0034-4257(01)00295-4).
- Friedl, M. A., D. Sulla-Menashe, B. Tan, A. Schneider, N. Ramankutty, A. Sibley, and X. M. Huang. 2010. "MODIS Collection 5 Global Land Cover: Algorithm Refinements and Characterization of New Datasets." *Remote Sensing of Environment* 114 (1): 168–182. doi:[10.1016/j.rse.2009.08.016](https://doi.org/10.1016/j.rse.2009.08.016).
- Gao, B.-C. 1996. "NDWI—A Normalized Difference Water Index for Remote Sensing of Vegetation Liquid Water from Space." *Remote Sensing of Environment* 58 (3): 257–266. doi:[10.1016/S0034-4257\(96\)00067-3](https://doi.org/10.1016/S0034-4257(96)00067-3).
- He, C. Y., P. J. Shi, D. Y. Xie, and Y. Y. Zhao. 2010. "Improving the Normalized Difference Built-Up Index to Map Urban Built-Up Areas Using a Semiautomatic Segmentation Approach." *Remote Sensing Letters* 1 (4): 213–221. doi:[10.1080/01431161.2010.481681](https://doi.org/10.1080/01431161.2010.481681).
- Huete, A. R. 1988. "A Soil-Adjusted Vegetation Index (Savi)." *Remote Sensing of Environment* 25 (3): 295–309. doi:[10.1016/0034-4257\(88\)90106-x](https://doi.org/10.1016/0034-4257(88)90106-x).
- Jia, M. M., Y. Z. Zhang, Z. M. Wang, K. S. Song, and C. Y. Ren. 2014. "Mapping the Distribution of Mangrove Species in the Core Zone of Mai Po Marshes Nature Reserve, Hong Kong, Using Hyperspectral Data and High-Resolution Data." *International Journal of Applied Earth Observation and Geoinformation* 33: 226–231. doi:[10.1016/j.jag.2014.06.006](https://doi.org/10.1016/j.jag.2014.06.006).
- Kauth, R. J., and G. S. Thomas. 1976. "The Tasseled Cap The Tasseled Cap - A Graphic Description of the Spectral-Temporal Development of Agricultural Crops as Seen by LANDSAT." *LARS Symposia* 159. http://docs.lib.psu.edu/lars_symp/159
- Kayabol, K. 2015. "Histogram-Based Contextual Classification of SAR Images." *Ieee Geoscience and Remote Sensing Letters* 12 (1): 33–37. doi:[10.1109/lgrs.2014.2325220](https://doi.org/10.1109/lgrs.2014.2325220).
- Kayadibi, Ö., and D. Aydal. 2013. "Quantitative and Comparative Examination of the Spectral Features Characteristics of the Surface Reflectance Information Retrieved from the Atmospherically Corrected Images of Hyperion." *Journal of Applied Remote Sensing* 7 (1): 073528. doi:[10.1117/1.jrs.7.073528](https://doi.org/10.1117/1.jrs.7.073528).
- Liu, X. Y., Y. Meng, A. Z. Yue, J. B. Chen, and Q. Q. Huang. 2014. "New Normalized Difference Index for Built-Up Land Enhancement Using Airborne Visible Infrared Imaging Spectrometer Imagery." *Journal of Applied Remote Sensing* 8 (1): 085092. doi:[10.1117/1.jrs.8.085092](https://doi.org/10.1117/1.jrs.8.085092).
- Loveland, T. R., B. C. Reed, J. F. Brown, D. O. Ohlen, Z. Zhu, L. Yang, and J. W. Merchant. 2000. "Development of a Global Land Cover Characteristics Database and IGBP Discovr from 1 Km AVHRR Data." *International Journal of Remote Sensing* 21 (6–7): 1303–1330. doi:[10.1080/014311600210191](https://doi.org/10.1080/014311600210191).
- Lu, D., and Q. Weng. 2007. "A Survey of Image Classification Methods and Techniques for Improving Classification Performance." *International Journal of Remote Sensing* 28 (5): 823–870. doi:[10.1080/01431160600746456](https://doi.org/10.1080/01431160600746456).
- Melgani, F., and L. Bruzzone. 2004. "Classification of Hyperspectral Remote Sensing Images with Support Vector Machines." *Ieee Transactions on Geoscience and Remote Sensing* 42 (8): 1778–1790. doi:[10.1109/tgrs.2004.831865](https://doi.org/10.1109/tgrs.2004.831865).
- Mozumder, C., N. K. Tripathi, and T. Tipdecho. 2014. "Ecosystem Evaluation (1989-2012) of Ramsar Wetland Deepor Beel Using Satellite-Derived Indices." *Environmental Monitoring and Assessment* 186 (11): 7909–7927. doi:[10.1007/s10661-014-3976-2](https://doi.org/10.1007/s10661-014-3976-2).
- Plaza, A., J. A. Benediktsson, J. W. Boardman, J. Brazile, L. Bruzzone, G. Camps-Valls, J. Chanussot, M. Fauvel, P. Gamba, A. Gualtieri, M. Marconcini, J. C. Tilton, and G. Trianni. 2009. "Recent Advances in Techniques for Hyperspectral Image Processing." *Remote Sensing of Environment* 113: SS110-SS122. doi:[10.1016/j.rse.2007.07.028](https://doi.org/10.1016/j.rse.2007.07.028).
- Powers, R. P., T. Hermosilla, N. C. Coops, and G. Chen. 2015. "Remote Sensing and Object-Based Techniques for Mapping Fine-Scale Industrial Disturbances." *International Journal of Applied Earth Observation and Geoinformation* 34: 51–57. doi:[10.1016/j.jag.2014.06.015](https://doi.org/10.1016/j.jag.2014.06.015).
- Ridd, M. K. 1995. "Exploring a V-I-S (Vegetation-Impervious Surface-Soil) Model for Urban Ecosystem Analysis through Remote Sensing: Comparative Anatomy for Cities†." *International Journal of Remote Sensing* 16 (12): 2165–2185. doi:[10.1080/01431169508954549](https://doi.org/10.1080/01431169508954549).
- Somers, B., G. P. Asner, L. Tits, and P. Coppin. 2011. "Endmember Variability in Spectral Mixture Analysis: A Review." *Remote Sensing of Environment* 115 (7): 1603–1616. doi:[10.1016/j.rse.2011.03.003](https://doi.org/10.1016/j.rse.2011.03.003).

- Song, H. H., B. Huang, Q. S. Liu, and K. H. Zhang. 2015. "Improving the Spatial Resolution of Landsat TM/ETM+ Through Fusion with SPOT5 Images via Learning-Based Super-Resolution." *Ieee Transactions on Geoscience and Remote Sensing* 53 (3): 1195–1204. doi:[10.1109/tgrs.2014.2335818](https://doi.org/10.1109/tgrs.2014.2335818).
- Swain, P. H., and S. M. Davis. 1981. "Remote Sensing: The Quantitative Approach." *IEEE Transactions on Pattern Analysis and Machine Intelligence* PAMI-3 (6): 713–714. doi:[10.1109/TPAMI.1981.4767177](https://doi.org/10.1109/TPAMI.1981.4767177).
- Tan, K., E. Li, Q. Du, and P. Du. 2014. "An Efficient Semi-Supervised Classification Approach for Hyperspectral Imagery." *Isprs Journal of Photogrammetry and Remote Sensing* 97: 36–45. doi:[10.1016/j.isprsjprs.2014.08.003](https://doi.org/10.1016/j.isprsjprs.2014.08.003).
- Thomas, I. L., N. P. Ching, V. M. Benning, and J. A. D'Aguanno. 1987. "Review Article A Review of Multi-Channel Indices of Class Separability." *International Journal of Remote Sensing* 8 (3): 331–350. doi:[10.1080/01431168708948645](https://doi.org/10.1080/01431168708948645).
- Varshney, A., and E. Rajesh. 2014. "A Comparative Study of Built-up Index Approaches for Automated Extraction of Built-up Regions from Remote Sensing Data." *Journal of the Indian Society of Remote Sensing* 42 (3): 659–663. doi:[10.1007/s12524-013-0333-9](https://doi.org/10.1007/s12524-013-0333-9).
- Weng, Q. H., X. F. Hu, and H. Liu. 2009. "Estimating Impervious Surfaces Using Linear Spectral Mixture Analysis with Multitemporal ASTER Images." *International Journal of Remote Sensing* 30 (18): 4807–4830. doi:[10.1080/01431160802665926](https://doi.org/10.1080/01431160802665926).
- Xu, H. 2006. "Modification of Normalised Difference Water Index (NDWI) to Enhance Open Water Features in Remotely Sensed Imagery." *International Journal of Remote Sensing* 27 (14): 3025–3033. doi:[10.1080/01431160600589179](https://doi.org/10.1080/01431160600589179).
- Xu, H. Q. 2010. "Analysis of Impervious Surface and its Impact on Urban Heat Environment using the Normalized Difference Impervious Surface Index (NDISI)." *Photogrammetric Engineering & Remote Sensing* 76 (5): 557–565. doi:[10.14358/PERS.76.5.557](https://doi.org/10.14358/PERS.76.5.557).
- Yang, L., S. V. Stehman, J. H. Smith, and J. D. Wickham. 2001. "Thematic Accuracy of MRLC Land Cover for the Eastern United States." *Remote Sensing of Environment* 76 (3): 418–422. doi:[10.1016/s0034-4257\(01\)00187-0](https://doi.org/10.1016/s0034-4257(01)00187-0).
- Yu, Q., P. Gong, N. Clinton, G. Biging, M. Kelly, and D. Schirokauer. 2006. "Object-Based Detailed Vegetation Classification with Airborne High Spatial Resolution Remote Sensing Imagery." *Photogrammetric Engineering & Remote Sensing* 72 (7): 799–811. doi:[10.14358/PERS.72.7.799](https://doi.org/10.14358/PERS.72.7.799).
- Yusuf, Y. A., B. Pradhan, and M. O. Idrees. 2014. "Spatio-temporal Assessment of Urban Heat Island Effects in Kuala Lumpur Metropolitan City Using Landsat Images." *Journal of the Indian Society of Remote Sensing* 42 (4): 829–837. doi:[10.1007/s12524-013-0342-8](https://doi.org/10.1007/s12524-013-0342-8).
- Zha, Y., J. Gao, and S. Ni. 2003. "Use of Normalized Difference Built-Up Index in Automatically Mapping Urban Areas from TM Imagery." *International Journal of Remote Sensing* 24 (3): 583–594. doi:[10.1080/01431160304987](https://doi.org/10.1080/01431160304987).
- Zhang, F., T. Tiyip, V. C. Johnson, H.-T. Kung, J.-L. Ding, Q. Sun, M. Zhou, A. Kelimu, I. Nurmuhamat, and N. W. Chan. 2015. "The Influence of Natural and Human Factors in the Shrinking of the Ebinur Lake, Xinjiang, China, during the 1972–2013 Period." *Environmental Monitoring and Assessment* 187 (1): 4128–4141. doi:[10.1007/s10661-014-4128-4](https://doi.org/10.1007/s10661-014-4128-4).
- Zhang, Y., H. Zhang, and H. Lin. 2014. "Improving the Impervious Surface Estimation with Combined Use of Optical and SAR Remote Sensing Images." *Remote Sensing of Environment* 141: 155–167. doi:[10.1016/j.rse.2013.10.028](https://doi.org/10.1016/j.rse.2013.10.028).
- Zhou, Y., G. Yang, S. Wang, L. Wang, F. Wang, and X. Liu. 2014. "A New Index for Mapping Built-Up and Bare Land Areas from Landsat-8 OLI Data." *Remote Sensing Letters* 5 (10): 862–871. doi:[10.1080/2150704X.2014.973996](https://doi.org/10.1080/2150704X.2014.973996).